Title

Surface control of Ni-Al2O3 dry reforming of methane catalyst by composition segregation

Authors

Kim, Min-Jae
Kim, Jeongmin
Kim, Yong Jun
et al.

Peer reviewed
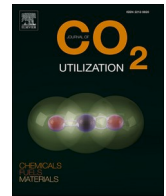
Surface control of Ni-Al$_2$O$_3$ dry reforming of methane catalyst by composition segregation

Min-Jae Kim [a,b,1], Jeongmin Kim [b,1], Yong Jun Kim [b], Jae-Rang Youn [c], Dong Hyun Kim [a,b], David Shapiro [a], Jinghua Guo [a,*], Kyubock Lee [a,b,**]

[a] Advanced Light Source, Lawrence Berkeley National Laboratory, Berkeley, CA 94720, USA
[b] Graduate School of Energy Science and Technology, Chungnam National University, 99 Daehak-ro, Yuseong-gu, Daejeon 34134, Republic of Korea
[c] Korea Institute of Energy Research, 152 Gajeong-ro, Yuseong-gu, Daejeon 34129, Republic of Korea

ARTICLE INFO

ABSTRACT

Catalyst surface control is of great importance considering that a catalytic reaction initially starts with surface atoms' interaction with reactant molecules. In the present study, we synthesized the Ni-Al$_2$O$_3$ dry reforming of methane (DRM) catalyst via the spray-pyrolysis-assisted evaporation-induced self-assembly (EISA) method in order to systematically investigate catalyst surface change as controlled by composition segregation. The present results showed that segregation in the Ni-Al$_2$O$_3$ catalyst had successfully occurred by the post-annealing process and that the segregated Ni nanoparticles were located on the catalyst surface with simultaneous reduction to metal. The size of the surface Ni nanoparticles was highly dependent on the post-annealing temperature, whereas the electronic properties did not consistently align with the trend of particle-size growth, indicating that the particle-growth mechanism underwent alterations from segregation to sintering as the temperature was increased. In other words, when the reduction temperature for metal segregation is excessively high, particle-growth on the external catalyst surface, as induced by post-annealing, is primarily attributable to particle sintering rather than to metal segregation. This phenomenon directly results in decreased Ni surface density. The catalytic DRM reaction revealed that due to sintering, the catalytic performance did not align with the trend of Ni particle-size growth, and the conversion of CH$_4$/CO$_2$ was closely associated with Ni surface density. This information will offer valuable insight to future research focused on development of Ni-based catalysts for DRM reactions.

1. Introduction

Catalyst surface control is of great importance considering that a catalytic reaction initially starts with surface atoms' interaction with reactant molecules [1]. However, precise control of the catalyst surface in the preparation of heterogeneous catalysts is challenging. Thus, interest in a catalyst synthesis method for easy catalyst surface control has grown [1,2]. In general, catalyst preparation involves several techniques such as co-precipitation, impregnation, and sol-gel methods [2,3]. Co-precipitation allows for precise control of metal content but is not so effective for particle-size and dispersion control; impregnation can easily prepare a layer of active matter on the catalyst surface but limits

the amount of active metal there [2,3]; the sol-gel method offers flexibility in the control of various parameters for management of catalyst particle size and dispersion [2,3]. However, during the thermal treatment process, significant volume shrinkage and cracking is incurred, which renders control of catalyst structure and shape difficult [2,3]. As such, despite the ongoing research into diverse catalyst synthesis methods, there still remain areas requiring further improvement for effective catalyst surface engineering.

There are noteworthy approaches to control the catalyst surface, namely, exsolution and segregation [1]. They are very similar concept and entails a phenomenon by which different atoms are enriched in different regions of well-mixed particles. They lead to decreased

solubility of one component, prompting the formation of a new solid phase within the original material and the creation of distinct regions or domains [1,4]. However, the segregation can be understood and interpreted with broader concept than the exsolution. The exsolution which can be described as the diffusion of metallic cations mainly happen in well-defined crystalline lattice structure such as perovskite and spinel, while the segregation which is wider concept including the exsolution covers element migration in homogeneous and inhomogeneous composition mixture [4]. In order to selectively manage composition segregation, precise control over both temperature and the atmosphere is essential during the post-annealing process [4]. This is crucial as composition segregation occurs only when there is a minimum overall Gibbs free energy, a condition met when the energy tending to segregation overwhelms that of chemical ordering [4]. The catalyst surface can be segregated by the heat treatment atmosphere into oxygen (O_2), carbon monoxide (CO), nitric oxide (NO), and hydrogen (H_2) [5–7]. In this context, one metal will more strongly interact with one adsorbate than with another, thereby leading to surface segregation [6,8]. Much effort has been devoted to the design and synthesis of nanomaterials via composition segregation, though they have focused mainly on positioning of a noble metal at certain locations as mixed with another noble or a transition metal (e.g. Rh-Pd [5], Au-Cu [9], Pd-Cu [7], and Pt-Ni [4]). Recently, trial investigations into induction of transition-metal-based catalysts by composition segregation without noble metal have been undertaken. For example, Weng et al. studied the structural changes occurring in the $NiCeO_2$ catalyst via composition segregation [9]. They insisted that by this method, Ni metals can be selectively positioned on the surfaces of oxide nanoparticles for simultaneous reduction to metal [9]. Moreover, their segregated $NiCeO_2$ catalyst promoted the catalytic reaction by facilitating water dissociation relative to an untreated $NiCeO_2$ catalyst, owing to the synergistic effects of the strong metal-support interaction [9]. Although other studies likewise have reported positive results for the catalytic reaction in the synthesis of transition-metal-based catalysts via composition segregation, there remains a scarcity of such examples without noble metal.

Dry reforming of methane (DRM), which converts CO_2 and CH_4 into valuable synthesis gases (CO and H_2), is a catalytic process providing strong economic and environmental incentives [10,11]. With regard to DRM catalysts, although noble metals have shown higher activity and stability than transition metals, their use is limited by their high cost and restricted availability on the commercial scale [12,13]. As an alternative to noble-metal catalysts, Ni-based catalysts, especially Al_2O_3-supported Ni catalysts with many active-metal, support, and promoter modifications, have been the focus in thousands of studies on DRM reaction [10, 11,14,15]. The main concerns of such research, however, have been the active sites that are determinative of catalytic mechanisms and activities; comparatively, there have been few attempts to reveal the relationship between Ni active-site number and catalytic efficiency [10,11, 14,15].

In the present study, the Ni-Al_2O_3 DRM catalyst was synthesized via the spray-pyrolysis-assisted evaporation-induced self-assembly (EISA) method in order to systematically investigate catalyst surface change as controlled by composition segregation. To obtain different sizes of Ni nanoparticles on the catalyst surface, we conducted post-annealing under an H_2 atmosphere with increasing temperature. The selection of Al_2O_3 for this Ni segregation study was driven by several considerations. Firstly, when two atoms of different sizes are placed in the same particle, the smaller atoms (Ni) are favorable to segregated nanostructure formation on the catalyst surface. Secondly, Al_2O_3 is characterized by its lower reducibility, making it a suitable choice to extract Ni from the complex composition of the catalyst. To facilitate the segregation of Ni, it's beneficial to have one well-reducible and one less-reducible material. Lastly, the pragmatic choice of Al_2O_3, a widely used material in dry reforming reactions, adds practical relevance to the study.

The catalyst samples were characterized for temperature-dependent Ni nanoparticle size/growth using scanning electron microscopy (SEM), transmission electron microscopy (TEM), and x-ray diffraction (XRD) analysis. Further, the physicochemical properties were analyzed using x-ray photoelectron spectroscopy (XPS) and ultraviolet-visible (UV–vis) spectroscopy. Our results revealed successful segregation through a post-annealing process that resulted in segregated Ni nanoparticles located on the catalyst surface with concurrent reduction to the metallic state. The size of the Ni nanoparticles on the catalyst surface was highly dependent on the post-annealing temperature, whereas the electronic properties did not consistently follow the particle-size growth trend. This was due to the particle-growth mechanism having undergone alterations from segregation to sintering as the temperature was increased, as confirmed by surface density calculations. To determine and examine the exact relationship between these changes and the efficiency of catalytic reactions, the samples were tested in DRM reactions. The results showed that the catalytic performance followed the trend of Ni surface density rather than that of Ni particle size, indicating that catalytic efficiency is determined by the number of active sites.

2. Experimental section

2.1. Materials

Nickel nitrate (Ni(NO_3)$_2$•6 H_2O, ≥ 98%, Sigma-Aldrich, St. Louis, Missouri, USA) and aluminum nitrate (Al(NO_3)$_3$•9 H_2O, ≥ 98%, Sigma-Aldrich) were used as sources of Ni and Al, respectively. Pluronic P123 triblock copolymer ($EO_{20}PO_{70}EO_{20}$, molecular weight = 5800 g/mol, Sigma-Aldrich) was employed as a structure-directing agent, and anhydrous ethanol (C_2H_5OH, ≥ 98%, Samchun Pure Chemical Co., Ltd.) and nitric acid (HNO_3, ≥ 60%, Samchun Pure Chemical Co., Ltd.) were used as dissolving agents. All of the materials were used as received without any further purification.

2.2. Catalyst synthesis using spray-pyrolysis-assisted EISA method

The Ni-Al_2O_3 catalyst was prepared by the spray-pyrolysis-assisted one-pot EISA method. First of all, 20 g of P123 were added to a solution consisting of 460 mL of D.I. water, 500 mL of ethanol, and 40 g of HNO_3, and then, stoichiometric quantities of Ni(NO_3)$_2$•6 H_2O and Al (NO_3)$_3$•9 H_2O (10 wt% metallic nickel balanced with aluminum oxide) were dissolved in the same solution (actual amount of Ni as confirmed by inductively coupled plasma optical emission spectroscopy (ICP–OES, OPTIMA8300, Perkin Elmer, MA, USA: 15.1 wt%). The well-mixed solution was moved to a spray vessel, and the mist was produced by a 1.7 MHz ultrasonic nebulizer with five piezoelectric vibrators. The mist was transferred by 5 L min^{-1} of N_2 gas flow into a tubular quartz reactor retaining a temperature of 700 °C by an electric furnace controlled with a thermocouple directly inserted into the middle of the quartz reactor. The pyrolyzed particles were collected by a back filter heated to 110 °C. Subsequently, the collected sample was calcined to 600 °C for 2 h at a ramping rate of 5 °C·min^{-1}.

2.3. Catalyst characterization

For characterizations, an as-calcined sample was reduced for 2 h to the desired temperature using 4% H_2 in N_2 balance at a ramping rate of 5 °C·min^{-1}. The crystal structure of the catalysts was probed using X-ray diffraction (XRD, D/MAX-2500, Rigaku, Corp., Japan) with a detector equipped with Cu-Kα radiation. Also, *in-situ* XRD spectra were recorded using a Rigaku X-ray diffractometer (D/ Max-III C, Rigaku, Corp., Japan) over the temperature range of 25 °C to 800 °C in a flow of 4% H_2 in Ar balance at a 2 °C·min^{-1} ramping rate. The scan range was 30 ° to 70 °, and the scanning speed was 6 °·min^{-1}. Brunauer–Emmett–Teller (BET) surface areas were determined from N_2 adsorption-desorption isotherms recorded at −196 °C (BELSORP-max, MicrotracBEL Corp., Osaka, Japan). The amount of Ni was measured by ICP-OES. Field-emission

scanning electron microscopy (FE-SEM) images were recorded to determine the catalyst surface using a Merlin compact (Carl Zeiss, Oberkochen, Germany). Transmission electron microscopy (TEM) images were obtained using a FEI Tecnai G2 F30 TEM (FEI Co., Hillsboro, OR, USA) at 300 keV, as equipped with an energy dispersive X-ray spectroscopy (EDS) detector with a Schottky field-emission-type electron source. H_2 temperature-programmed reduction (H_2-TPR) experiments were performed using an Autochem 2950 HP instrument (Micromeritics Instrument Corp., Norcross, GA, USA). In the H_2–TPR experiment, 100 mg of sample was loaded onto a quartz tube and pretreated under a flow of 10% O_2 in He, at 200°C for 1 h. After pretreatment, the TPR experiments were carried out in the temperature range of 50 – 1000 °C, using 10% H_2/Ar at a ramping rate of 2 °C·min^{-1}. A UV–vis diffuse reflectance spectroscopy (UV–vis DRS) experiment was performed with an S-3100 (SCINCO, Seoul, South Korea.). For precise analysis, Barium sulfate ($BaSO_4$, > 99%, Sigma-Aldrich) was used as the reference spectra. X-ray photoelectron spectroscopy (XPS) was performed using an ESCALAB Mk II spectrometer (VG Scientific, Ltd. Cambridge, UK) with Al Kα radiation (hv = 1486.6 eV) at constant energy of 50 eV. The binding energies were aligned based on the C 1 s line at 284.6 eV originating from adventitious carbon. A thermogravimetric (TG) analysis was carried out using a TGA N-1000 instrument (SCINCO, Seoul, South Korea) under air flow at a heating rate of 10 °C·min^{-1}.

2.4. Catalytic activity evaluation

The catalytic reaction was performed under atmospheric pressure in a fixed-bed reactor using a quartz tube of 4 mm internal diameter, and the reaction temperature was controlled with a thermocouple located at the center of the catalyst bed. Before the reaction was initiated, the catalyst was pretreated with H_2 at each temperature for 2 h. The DRM reaction was performed at 700°C with a feed gas in a 1:1:1 ratio of CH_4: CO_2: N_2 at 180,000 mL·$g_{cat}^{-1}h^{-1}$ weight hourly space velocity (WHSV). The product gas from the reactor was recorded by micro gas
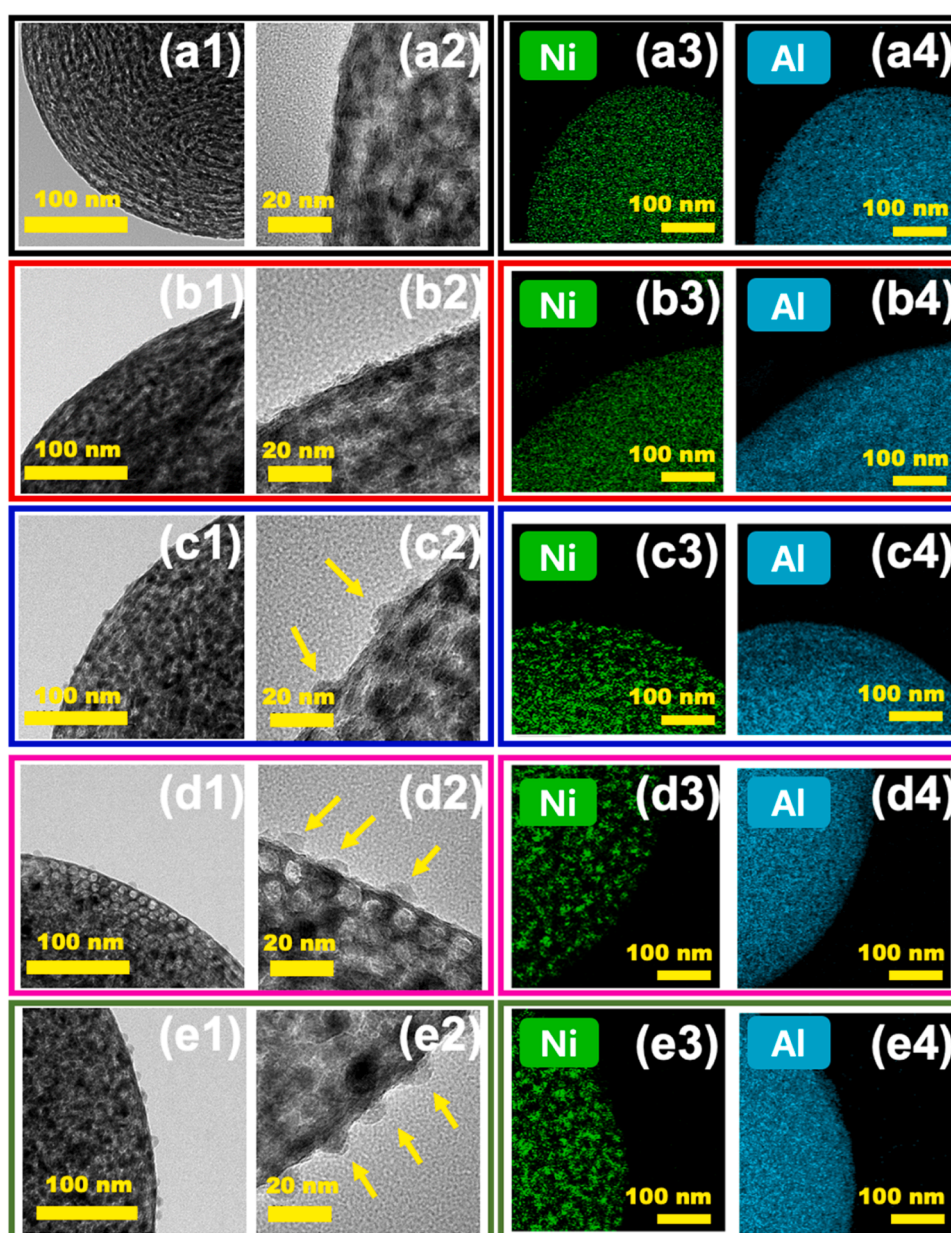
Fig. 1. TEM and EDS mapping images of as-calcined (NiAl-cal (a)) and reduced (NiAl-500 (b), NiAl-600 (c), NiAl-700 (d), and NiAl-800 (e)) catalysts; (a1 – e1) for 100 nm scale bar, (a2 – e2) for 20 nm scale bar, (a3 – e3) for Ni element, and (a4 – e4) for Al element.

chromatography (Inficon 3000, INFICON Inc., CA, USA). The conversions of CO_2/CH_4 and the H_2/CO ratio were defined as follows:

$$CO_2 \text{ conversion } (\%) = \frac{[CO_2]_{in} - [CO_2]_{out}}{[CO_2]_{in}} \times 100$$

$$CH_4 \text{ conversion } (\%) = \frac{[CH_4]_{in} - [CH_4]_{out}}{[CH_4]_{in}} \times 100$$

$$H_2 \Big/ CO \text{ ratio} = \frac{[H_2]_{out}}{[CO]_{out}}$$

where $[CH_4]_{in}$ and $[CO_2]_{in}$ correspond to the concentrations of CH_4 and CO_2 at the reactor inlet, respectively, and $[CH_4]_{out}$, $[CO_2]_{out}$, $[H_2]_{out}$, and $[CO]_{out}$ correspond to the concentrations of CH_4, CO_2, H_2, and CO at the reactor outlet, respectively.

3. Results and discussion

3.1. Structural and morphological evolution observation

The morphology of all the samples synthesized by the spray-pyrolysis-assisted EISA method was identical regardless of whether they had been calcined or reduced, showing a spherical shape and a catalyst particle size of 0.5 – 2 μm (Figure S1). One particle is formed from one droplet of aqueous precursor that is generated by an ultrasonic atomizer, the spherical shape of the particles originating from rapid solvent evaporation and pyrolysis of precursor droplets during the synthesis procedure [16,17]. As for the as-calcined sample in Fig. 1 (a1–a4), TEM and EDS mapping images show one catalyst particle having the well-developed pore structure layer by layer. Note also that two elements (Ni and Al) are located at the same position, indicating the well-distributed composition in the Ni-Al$_2$O$_3$ catalyst. This was owed to the fact that the spray-pyrolysis method produces catalyst particles with a homogeneous distribution of heteroatoms via kinetic quenching, which is mediated by a few seconds of fast drying to pyrolysis [16,17]. In the case of the as-reduced samples, the NiAl-500 catalyst having the partially reduced Ni species had an uneven surface with a few changes, but the elemental locations of Ni and Al were hardly changed (Fig. 1 (b1–b4)). The observable changes were detected in the NiAl-600, NiAl-700, and NiAl-800 catalysts (Fig. 1(c–e)). Several nanoparticles segregated from the Ni-Al$_2$O$_3$ particle were clearly shown, and moreover, nickel and aluminum were no longer homogeneously distributed in one catalyst particle. The Ni was the agglomerated element on the catalyst surface, and was gradually well developed with increasing reduction temperature, while the Al was positioned at the same location and did not move even at high reduction temperature.

The catalyst surface observed by SEM analysis exhibited significant differences as the reduction temperature was increased, as in the TEM analysis. The as-calcined sample, shown in Fig. 2(a), had a smooth surface without any segregated particles, because the two elements were well mixed in one catalyst particle. On the other hand, the as-reduced samples clearly had nanoparticles on the catalyst surface, as seen in Fig. 2(b-e). These nanoparticles were confirmed as nickel, based on the TEM-EDS mapping analysis, indicating that the locations of Ni and Al were distinguishable due to the metal segregation in one catalyst particle. The XRD pattern of the NiAl-cal catalyst exhibits very weak but characteristic peaks corresponding to NiO (PDF #44–1159) at 37.2 °,
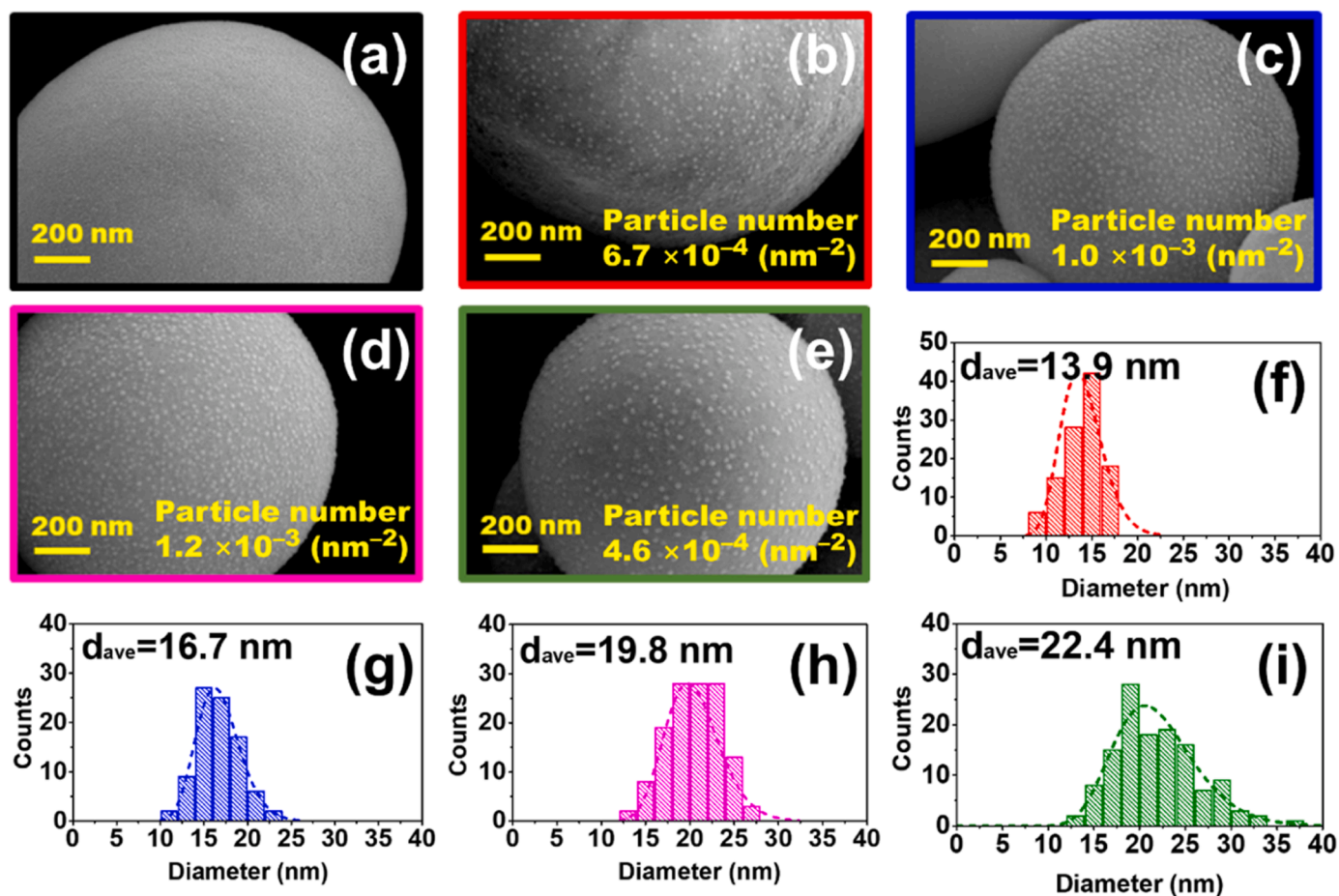
Fig. 2. SEM images of as–calcined (NiAl-cal (a)) and reduced (NiAl-500 (b), NiAl-600 (c), NiAl-700 (d), and NiAl-800 (e)) catalysts, respectively, and histograms of particle-size distribution for as–reduced (NiAl-500 (f), NiAl-600 (g), NiAl-700 (h), and NiAl-800 (i)) catalysts.

43.2 °, and 62.9 ° (Figure S2) [18,19]. After reduction at 500 °C, the main peak shifted from 43.3 ° (NiO) to 44.3 ° (Ni, PDF #65–2865), and two weak peaks corresponding to Ni were newly observed at 51.6 ° and 76.3 ° (Figure S2). The formation of the Ni phase became clearer for NiAl-600, for which the main peak of Al$_2$O$_3$ (PDF #29–0063) at 66.5 °, too, started to be shown [18,19]. Finally, in the NiAl-800 catalysts, the Ni and Al$_2$O$_3$ phases were individually formed, clearly demonstrating the segregation between Ni and Al$_2$O$_3$ (Figure S2). The size distribution of the segregated Ni nanoparticles, as measured based on the SEM images, is shown in Fig. 2(f–i): the average particle size of metallic Ni gradually increased from 13.9 nm to 22.4 nm as the reduction temperature was increased from 500 to 800 ºC. Table 1 depicted the change of Ni particle size measured by both SEM and *ex-situ* XRD, having the same tendency to be increased. However, there was a difference in the actual size change of Ni nanoparticles between SEM and *ex-situ* XRD because of the Pt coating for SEM analysis with a 7 – 8 nm of thickness. If consider this factor, the size change would be almost same. In the case of particle number on catalyst surface, it was increased from 6.7×10^{-4} (NiAl-500) to 1.2×10^{-3} (NiAl-700) nm^{-2} but was decreased to 4.6×10^{-4} nm^{-2} with further increasing the temperature to 800 °C. Namely, the number of Ni particles in the temperature range of 500 – 700 °C was increased by the growth and the new formation of Ni particles caused by the surface segregation. Thereafter, with further temperature increase, the particles were grown by merging the small particles, which results in the reduction of the number of particles. It indicates a sequential development of metallic Ni particles as follows: the reduction from NiO to Ni between 500 °C and 600 °C, the growth and the new formation of Ni particles by the surface segregation thereafter, and finally the growth of Ni particles by sintering at around 800 °C.

According to the literature, one of the parameters contributing to such composition segregation is the atomic radius of metals [4,21,22]. When two atoms of different sizes are placed in the same particle, strain is created due to the size mismatch, leading to compressive strain for larger atoms (atomic radius of Al: 143 pm) and tensile strain for smaller atoms (atomic radius of Ni: 124 pm) [4,21,22]. Thus, owing to this reason, the smaller atoms (Ni) would be shifted to the catalyst surface to form composition–segregated nanostructures, well corresponding to our samples [4]. This indicated that the metal–segregation had occurred in the homogeneously mixed composition and, further, that reduction temperature is a crucial factor for the metal–segregation phenomenon and determination of segregated metal size.

During Ni segregation, a change in pore structure also is expected. Hence, the N$_2$ adsorption-desorption technique was performed over as-calcined and as-reduced samples. Figure S3 illustrates the nitrogen adsorption/desorption isotherm and pore-size distribution of samples. As presented in Figure S3(a), all of the samples had a typical Type–IV

isotherm (as defined by IUPAC) with an evident hysteresis in a change of 0.6 – 0.9 P/P_0, indicating that the catalysts had a well-developed pore structure after the reduction treatment. The pore-size distribution of each sample was measured by the Barrett–Joyner–Halenda (BJH) method, as shown in Figure S3(b). All of the samples had pore sizes varying in the range of 2 – 30 nm (mesopores). The sole point of concern regarding the metal segregation was the destruction of the skeletal mesopores and structure, but this result clearly indicated that the well–defined mesopores did not collapse, even after the thermal and reduction treatment. Table 1 summarizes the BET surface area and total pore volume data.

The composition segregation was conducted under a hydrogen atmosphere. For a better understanding of structure change and segregation, we performed real-time phase changes for metal segregation over the Ni-Al$_2$O$_3$ catalyst, as characterized by H$_2$-TPR and *in-situ* XRD analyses. First, the H$_2$-TPR analysis showed the H$_2$ consumption reflective of the reduction behavior of NiAl-cal with increasing temperature (Figure S4). The H$_2$-TPR profile exhibited a strong H$_2$ consumption peak at 569 °C, which was ascribed to the reduction of the NiO clusters [23]. A small peak that appeared at 353 °C was attributed to the free NiO species, and the tailing peak corresponded to the reduction of NiO, which was relatively strongly bonded to Al$_2$O$_3$ [23]. The *in-situ* XRD analysis, performed in the H$_2$ atmosphere with increasing temperature from 25 to 800 °C at a ramping rate of 2 °C·min^{-1}, showed the temperature sequence of the XRD profiles covering the 2θ range from 30 ° to 70 ° (Figs. 3(a) and 3(b)). The main peak at 43.3°, assigned to the NiO phase, was shifted to 44.3 °, assigned to the main peak of a face–centered cubic Ni phase between 540 °C and 580 °C [18,19]. This temperature of phase transition closely matched the temperature of the highest reduction peak in the H$_2$-TPR analysis (Figure S4). Fig. 3(c) plots the crystal sizes and lattice constants of the NiO and metallic Ni with respect to temperature. The crystal size of NiO and metallic Ni was calculated based on the peaks of 43 ° and 51 °, respectively, and the planes of NiO (200) and Ni (111) were used for lattice constant measurement. The crystal size of the NiO phase increased slowly from 25 °C to 540 °C, whereas that of metallic Ni grew relatively fast from 580 °C to 800 °C. Moreover, the lattice constant was drastically changed in the temperature range of 500 – 600 °C, directly reflecting the phase transition from NiO to Ni^0 caused by the removal of the oxygen atoms. This thermal growth of particles and lattice expansion/shrinkage with temperature increase is considered to be key evidence of Ni segregation from the crystal structure [4,21,22].

In the light of the combined results of TEM-EDS mapping, SEM, and *in-situ* XRD analyses, it was concluded that composition segregation in Ni-Al$_2$O$_3$ had successfully occurred via the post-annealing process under the H$_2$ atmosphere; moreover, the particle-size growth of metallic Ni from 13.9 nm to 22.4 nm was clearly observed as the reduction temperature was increased from 500 to 800 °C. This indicates that the samples induced by the present composition segregation embodied a strong correlation between reduction temperature and particle size. Based on H$_2$-TPR and in-situ XRD analyses, furthermore, we speculate a sequential development of metallic Ni particles as follows: the reduction from NiO to Ni between 500 °C and 600 °C, the growth and the new formation of Ni particles by the surface segregation thereafter, and finally the growth of Ni particles by sintering at around 800 °C. The sintering is differentiated from the segregation in that the particles are grown by merging the small particles, which results in the reduction of the number of particles.

The surface electronic states and atomic concentrations of Ni, Al, and O in the as-calcined and reduced samples were investigated by XPS analysis (Fig. 4(a–c)). Curve–fitting for this analysis was performed after Shirley–type background subtraction using a combination of Gaussian and Lorentzian functions. For precise comparison, the XPS results for the NiAl-cal sample also are plotted. Fig. 4(a) presents the Ni 2p$_{3/2}$ spectra for the samples. The as-calcined sample presents only the two peaks at 855.3 and 861.4 eV ascribed to Ni^{2+} and the satellite peak, respectively

Table 1

Characteristics of as-prepared catalysts.

Samples	BET surface area^a [m^2 g^{-1}]	Total pore volume^a [cm^3 g^{-1}]	Ni particle size^b [nm]		Reduction degree^c (%)	Surface density of Ni^d [nm^{-2}]
			SEM	*Ex-situ XRD*		
NiAl-cal	122.32	0.5740				
NiAl-500	138.43	0.6455	13.9	6.8	23.9	1.77
NiAl-600	114.59	0.4650	16.7	9.6	66.1	5.92
NiAl-700	107.4	0.4444	19.8	13.1	90.4	8.64
NiAl-800	151.69	0.6480	22.4	15.2	98.7	6.68

^{a} Estimated from N$_2$ adsorption at −196°C. ^{b} Estimated from SEM and *ex-situ* XRD experiments. ^{c} Estimated from H$_2$-TPR. ^{d} Surface density of Ni (nm^{-2}) = (Ni content × Avogadro's number × reduction degree)/(molecular weight of Ni × BET surface area × 10^{-18}).
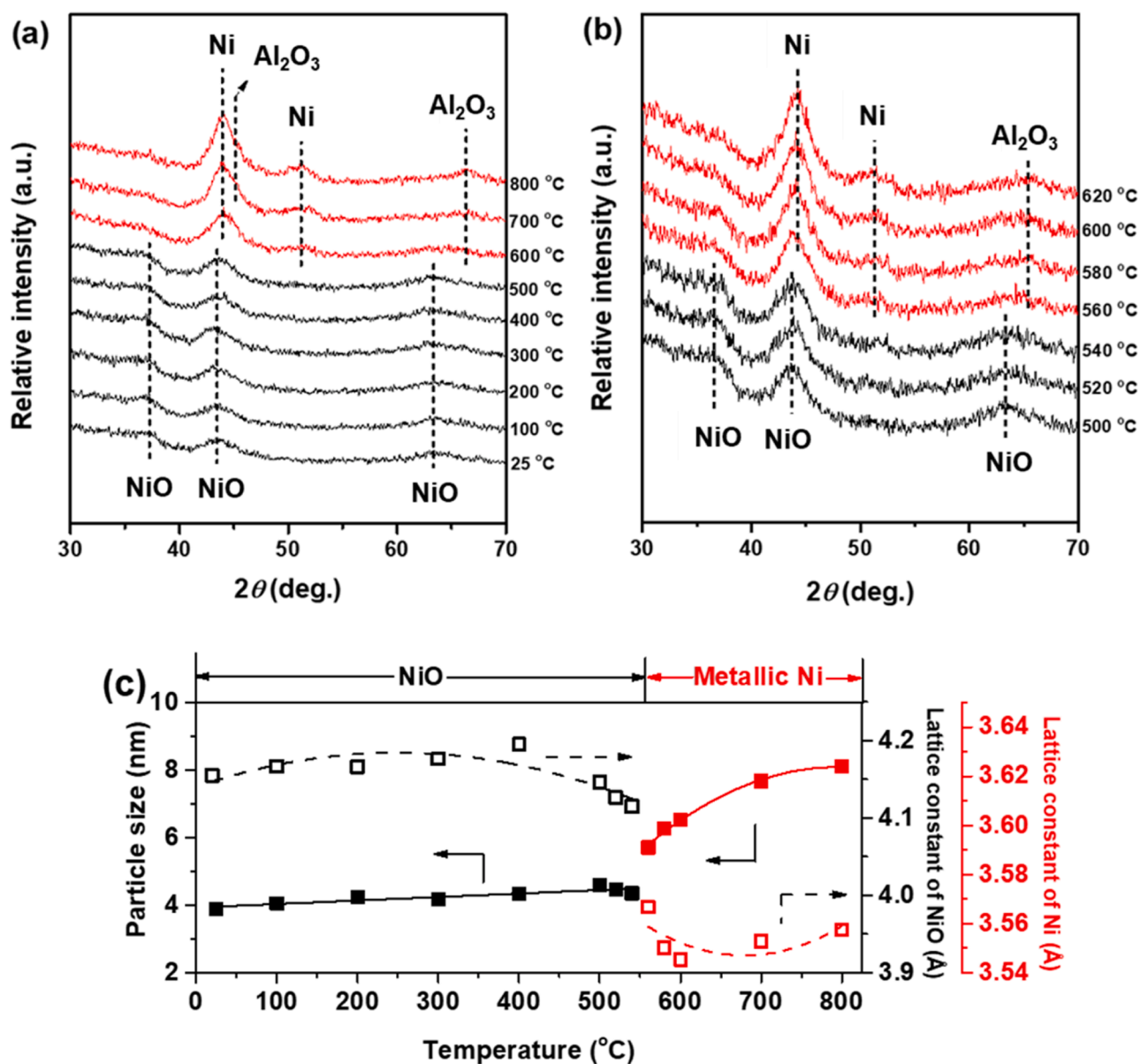
Fig. 3. *In-situ* X-ray diffraction patterns of Ni-Al$_2$O$_3$ catalyst (NiAl-cal) in 25 – 800°C range at intervals of 100°C (a) and in 500 – 620°C range at intervals of 20°C (b). Change of Ni/NiO particle size and Ni/NiO lattice constant as function of reduction temperature (c). Experimental conditions: 5% H$_2$ in Ar balance with ramping rate of 2°C·min^{-1}.

[18,24]. Other than these two peaks, a peak attributed to Ni^0 was newly observed at 852 eV in the as-reduced samples, and further, it was confirmed that the overall shape of the Ni 2p$_{3/2}$ spectra had changed according to the reduction temperature. This result clearly indicates that reduction temperature is one of the crucial factors for control of the amount of Ni^0 species. The relative concentrations of the Ni^0 species are summarized in Table 2. As the reduction temperature was increased from 500 to 700 °C, the concentrations increased from 12.6% to 38.2%, and the concentration of Ni^0 in the sample reduced at 800 °C decreased to 31.4%. In addition, the peak position of Ni^{2+} was shifted to a lower binding energy (BE), from 855.5 to 854.8 eV, as the reduction temperature was increased from 500 to 700 °C. In the case of NiAl-800, the BE moved to a higher energy, 855.4 eV. This result implies that the metal-support interaction of the catalysts tended to dwindle with the increase of reduction temperature from 500 to 700 °C, but that it was briefly strengthened when the reduction temperature reached 800 °C. Fig. 4(b) plots the Al 2p and Ni 3p spectra for the samples. All of the samples showed a single peak at 74.0 eV corresponding to Al^{3+} in Al 2p

[25,26]. Next to this Al 2p spectra, there was an additional peak at 67.9 eV assigned to Ni^{2+} in Ni 3p [27]. As the reduction temperature was increased, it became evident that this peak had undergone a noticeable shift towards a lower BE and became less pronounced. This result reflected the reduction process of Ni^{2+} to Ni^0. The O 1 s spectra of the samples are plotted in Fig. 4(c). All of the catalysts exhibited three well-defined peaks in the O 1 s spectra located at around 528.8, 530.5 and 532.5 eV. The one at 530.5 eV was ascribed to the Al–O bond (O$_{Al-O}$), and the other, observed at 530.5 and 532.5 eV, was attributed to the Ni–O bond (O′$_{Ni-O}$ and O''$_{Ni-O}$, respectively) [27,28]. O$_{Ni-O}$ includes all Ni atoms in different states attached with oxygen; similarly, O$_{Al-O}$ is associated with oxygen and Al bonding in all forms [28]. The peak position of the as-reduced samples was changed relative to that of NiAl-cal, and furthermore, the peak ratio of O$_{Ni-O}$ highly varied depending on the reduction temperature. These changes indicate that oxygen attached to Ni either was shifted to Al atoms or removed from the catalyst surface [28]. The ratios of O$_{Ni-O}$ and O$_{Al-O}$ were calculated through peak fitting and with reference to the areas under the fitted components, and are
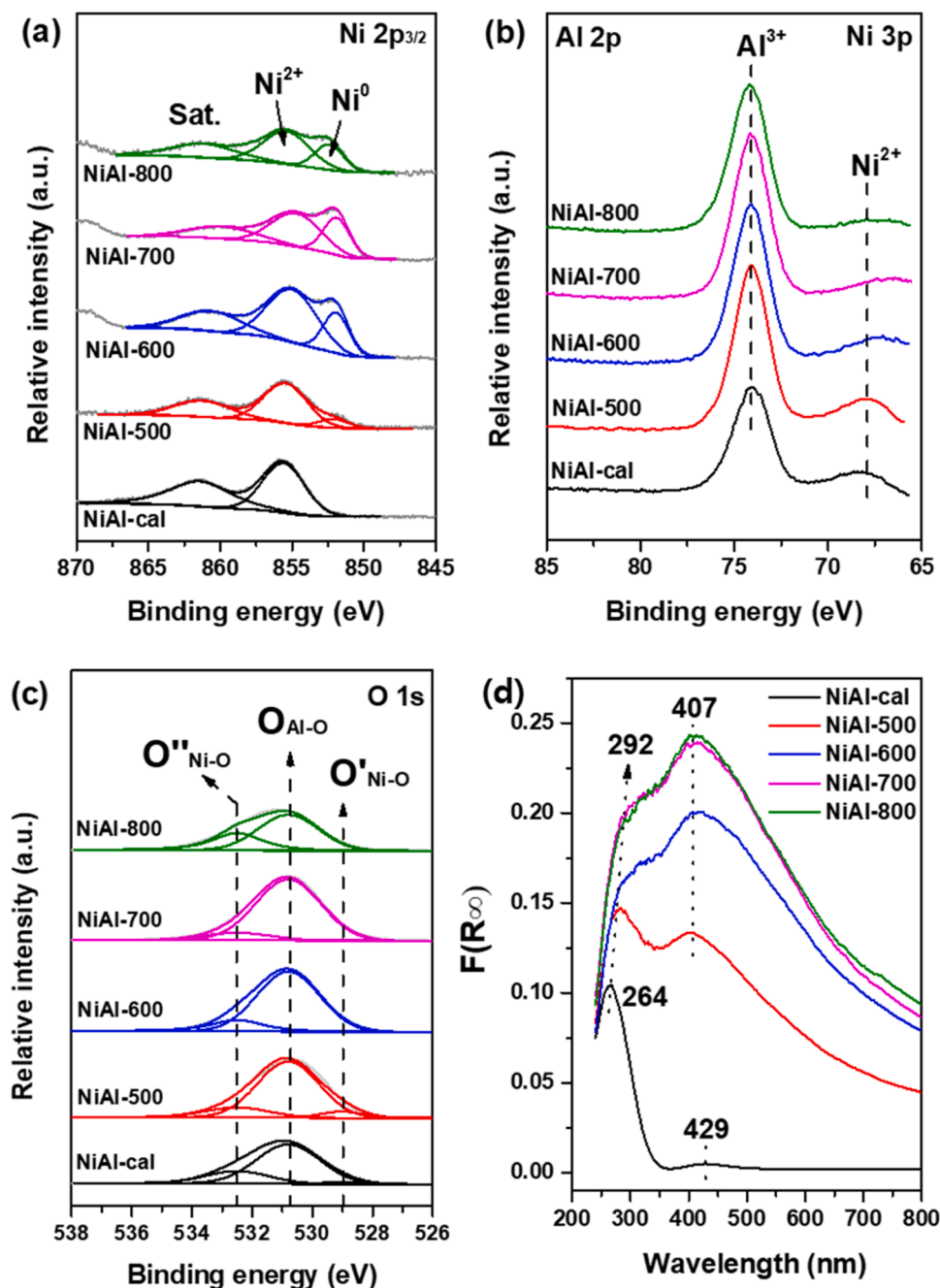
Fig. 4. X-ray photoelectron spectroscopy (XPS) of Ni $2p_{3/2}$ (a), Al 2p with Ni 3p (b), and O 1 s (c). UV–vis DRS of as-calcined and as-reduced samples (d).

summarized in Table 2. For the as-calcined sample, the amount of O_{Ni-O} was 42.2%. As the reduction temperature was increased to 700°C, the relative concentration of O_{Ni-O} decreased to 13.8%, as indicative of Ni–O bond disconnection and formation of the Al–O bond due to Ni segregation. However, the concentration of O_{Ni-O} in NiAl-800 increased to 25.1%. This result implies that a new interaction between Ni and O was formed at 800 °C and that this was one of the reasons for the decrease of the concentration of Ni^0 species as well as the peak shift toward higher BE in the Ni $2p_{3/2}$ spectra [27,28]. The change of electron transfer in accordance with the reduction temperature also was corroborated by UV–vis analysis. Fig. 4(d) plots the corresponding UV–vis spectra of the as-reduced samples, along with that of the as-calcined sample as a reference. One of the main bands of the NiAl-cal catalyst appeared at around 264 nm and was attributed to a charge transfer band from O^{2-} to octahedral Ni^{2+}; meanwhile, the other weak band at 429 nm

corresponded to the electron transition in the d-d orbital [29–31]. In the case of the as-reduced samples, however, a further red shift of the band to 292 nm as a result of the increasing reduction temperature indicated that the catalyst with metal segregation required less energy for charge transition from oxygen to transition metal [29–33]. A strong band attributed to the d – d transition was observed at ca 400 – 430 nm in the as-reduced catalysts, and moreover, it was confirmed that the overall shape of the UV–vis band had changed with reduction temperature, due specifically to the surface plasmonic resonance effect [29]. This change was caused by the segregated metal nanoparticles and abundant free electrons on the catalyst surface [29]. Despite the linear increase in the reduction temperature, there was little difference between NiAl-700 and NiAl-800 in UV–vis band. This suggests that the number of free electrons induced by the metal segregation already reached the maximum at the reduction temperature of 700 °C.

Table 2

Surface atomic ratios and binding energies of Ni and O species obtained by X-ray photoelectron spectroscopy (XPS).

Samples	Linear combination fitting area of XPS spectra		Relative concentration of Ni^0/Ni$_{total}$ (%)	Binding energy (eV)	
	Ni^0	Ni^{2+}		Ni^0	Ni^{2+}
NiAl-cal	-	37164.6	-	-	855.6
NiAl-500	2352.4	16179.6	12.6	851.9	855.5
NiAl-600	20505.0	48628.5	29.6	851.9	855.1
NiAl-700	21110.9	22320.2	38.2	851.9	854.8
NiAl-800	8500.2	12029.8	31.4	852.3	855.4

Samples	Linear combination fitting area of XPS spectra			Relative concentration of (O'$_{Ni-O}$+ O''$_{Ni-O}$)/O$_{total}$ (%)	Binding energy (eV)		
	O'$_{Ni-O}$	O''$_{Ni-O}$	O$_{Al-O}$		O'$_{Ni-O}$	O''$_{Ni-O}$	O$_{Al-O}$
NiAl-cal	6244.3	50452.6	166122.9	25.4	528.8	532.5	530.6
NiAl-500	18986.6	53434.0	227089.5	24.5	528.9	532.4	530.6
NiAl-600	4590.9	45009.25	248722.7	16.6	531.9	532.4	530.5
NiAl-700	5927.8	32819.9	264018.4	12.7	532.3	532.5	530.7
NiAl-800	-	81499.2	141738.9	36.5	-	532.5	530.6

Although the particle size, confirmed by XRD and SEM, increased linearly as the reduction temperature was increased, no linear change was observed in the electronic properties by XPS or UV–vis. We believed that there is a reason other than composition segregation for the particle-size increase. According to the literature, the sintering of Ni nanoparticles in Ni-Al$_2$O$_3$ catalyst can occur under a reduction atmosphere at high temperature (above 750 °C) [19,34]. Based on this fact, we applied a new strategy for this catalyst, entailing calculation of the surface density of Ni, to confirm either Ni segregation or Ni sintering. As the surface density of Ni represents the number of Ni atoms, the active metal in metallic Ni, on the surface of the support per unit specific surface area [35], Ni surface density was estimated according to the equation

$$n_s \quad (Ni \quad nm^{-2}) = \frac{c_w N_A}{M_w S_{BET} \times 10^{18}(nm^2 \bullet m^{-2})} \times R.D.$$

where c_w (g/g) is the Ni content of the catalysts, N_A the Avogadro's number (6.022 $\times$ 10^{23} mol^{-1}), M_w the molecular weight of Ni (58.69 g·mol^{-1}), S_{BET} (m^2·g^{-1}) the surface area of the catalysts, and *R.D.* the reduction degree by H$_2$-TPR analysis. The relationship of Ni particle size to estimated Ni surface density is given in Table 1. As shown, the particle size of Ni linearly increased with increased reduction temperature, while the surface density increased to the reduction temperature of 700 °C but decreased from 800 °C. Notably, the XPS data was well correspondent. With increasing reduction temperature to 700 °C, the metallic Ni species concentration was increased and that of O$_{Ni–O}$ was decreased, due to Ni segregation. With further increase of reduction temperature, however, Ni sintering occurred, leading to decreased metallic Ni and increased Ni–O bonding [36]. These results, confirmed by XRD, UV–vis, surface density, and XPS analysis, strongly support the finding that the size growth of Ni nanoparticles caused by Ni segregation in the Ni-Al$_2$O$_3$ catalyst took place in the temperature regime of 500–700 °C but that the Ni nanoparticles in the NiAl-800 catalyst were further grown by the sintering effect [19,34].
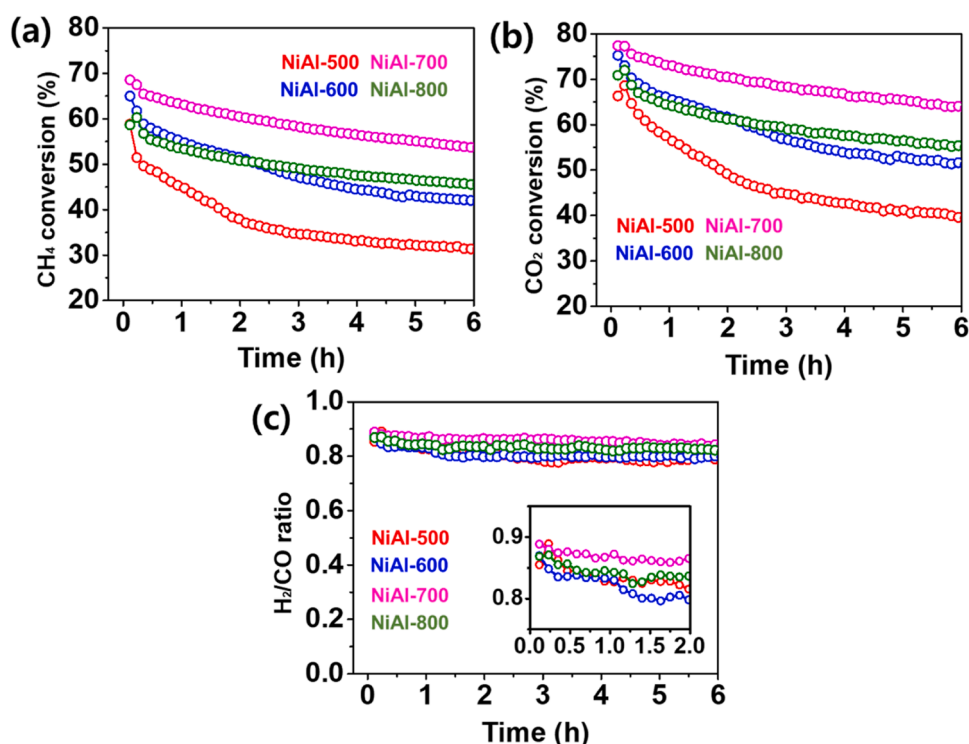
Fig. 5. CO$_2$ (a) and CH$_4$ (b) conversion and H$_2$/CO ratio of catalyst (c); Reaction conditions: T = 700°C, CH$_4$: CO$_2$: N$_2$ = 1:1:1, and WHSV = 180,000 mLg$_{cat}^{-1}$h^{-1}.

3.2. Catalytic evaluations for DRM reaction

In order to understand how this catalyst influences the catalytic reaction, the samples were applied to a DRM reaction. The reaction tests were carried out at 700 °C with a methane/carbon dioxide ratio (CH_4/CO_2) of 1 at 180,000 mL·g_{cat}^{-1} h^{-1} of WHSV to evaluate the catalytic activities over a series of metal-segregated samples. Fig. 5 plots the conversion of CH_4/CO_2 and the H_2/CO ratio over the NiAl-500, NiAl-600, NiAl-700, and NiAl-800 catalysts. For the conversion of CH_4 and CO_2, as displayed in Figs. 5(a) and 5(b), the conversion of CH_4/CO_2 was increased with the reduction temperature increase from 500–700 °C. With further increase of reduction temperature, however, the NiAl-800 catalyst showed low CH_4/CO_2 conversion. Fig. 5(c) presents the H_2/CO ratio for a series of as-segregated samples. All the catalysts maintained their H_2/CO ratio, with minor fluctuations, during the acceleration test. Among the metal-segregated catalysts, the NiAl-700 catalyst exhibited the highest H_2/CO ratio (approx. 0.87%). This result suggests that there is an optimum temperature (or active metal size) for metal segregation in the Ni-Al_2O_3 catalyst in terms of initial conversion of CH_4/CO_2, and that this metal segregation influences the kinetic mechanism of the DRM reaction.

There are many catalyst combinations for coke resistance during DRM reaction, such as Mg as a promoter, but in this study, we chose the simple Ni-Al_2O_3 catalyst to focus on the parameters such as particle size, Ni surface density, and catalytic performance. Thus, the coke deposition on the catalyst surface was an expected result and a more detailed characterization and discussion on the spent catalysts is available in Supplementary Information.

The physicochemical properties and reaction results, shown in Figs. 6(a) and 6(b), respectively, were compared to confirm the overall correlations. The TEM, SEM, and XRD analyses clearly indicated that the

segregated Ni nanoparticles were on the catalyst surface and were simultaneously reduced to the metallic state of Ni. Further, the particle size of Ni was gradually increased with increasing reduction temperature via composition segregation, indicating that the Ni particle size of the Ni-Al_2O_3 catalyst is highly dependent on reduction temperature. However, the electronic characteristics showed a different pattern. The concentration of metallic Ni did not exhibit any linear increase, and the number of free electrons capable of reacting with the reactant were not increased, when the temperature was increased from 700 to 800 °C, thus confirming that there was no additional composition segregation. Moreover, considering the surface density change along with the increase in O_{Ni-O} concentration at 800 °C, this can be interpreted as particle growth resulting from sintering phenomena rather than particle growth due to composition separation. Upon testing the catalyst subjected to post-annealing in the DRM reaction, it was observed that the initial conversion of CH_4/CO_2 did not exhibit the same trend as did Ni particle-size growth. The Ni particle-size growth in the reduction temperature range of 500 – 700 °C was gradually increased, leading to an increased number of active sites and achieving high initial conversion of CH_4/CO_2 thereby. However, the further development of Ni particles in the NiAl-800 catalyst resulted in a decline of the initial conversion due to the decreased active-site surface density and metallic Ni concentration accompanying the sintering [19–35]. In other words, the initial conversion of CH_4/CO_2 is more closely related to the surface density of Ni (i. e., the number of active sites) than to particle size. The coke formation was attributed to O 1 s: the surface lattice oxygen (O_α) at 530.6 eV and the chemisorbed oxygen (O_β) at 532.5 eV. According to the literature, O_β can supply more oxygen vacancies favorable for elimination of deposited coke and enhancement of catalytic stability [10]. As shown in Fig. 6 (b), the coke content was in inverse proportion to the concentration of O_β as induced by the composition segregation, and NiAl-700 with the
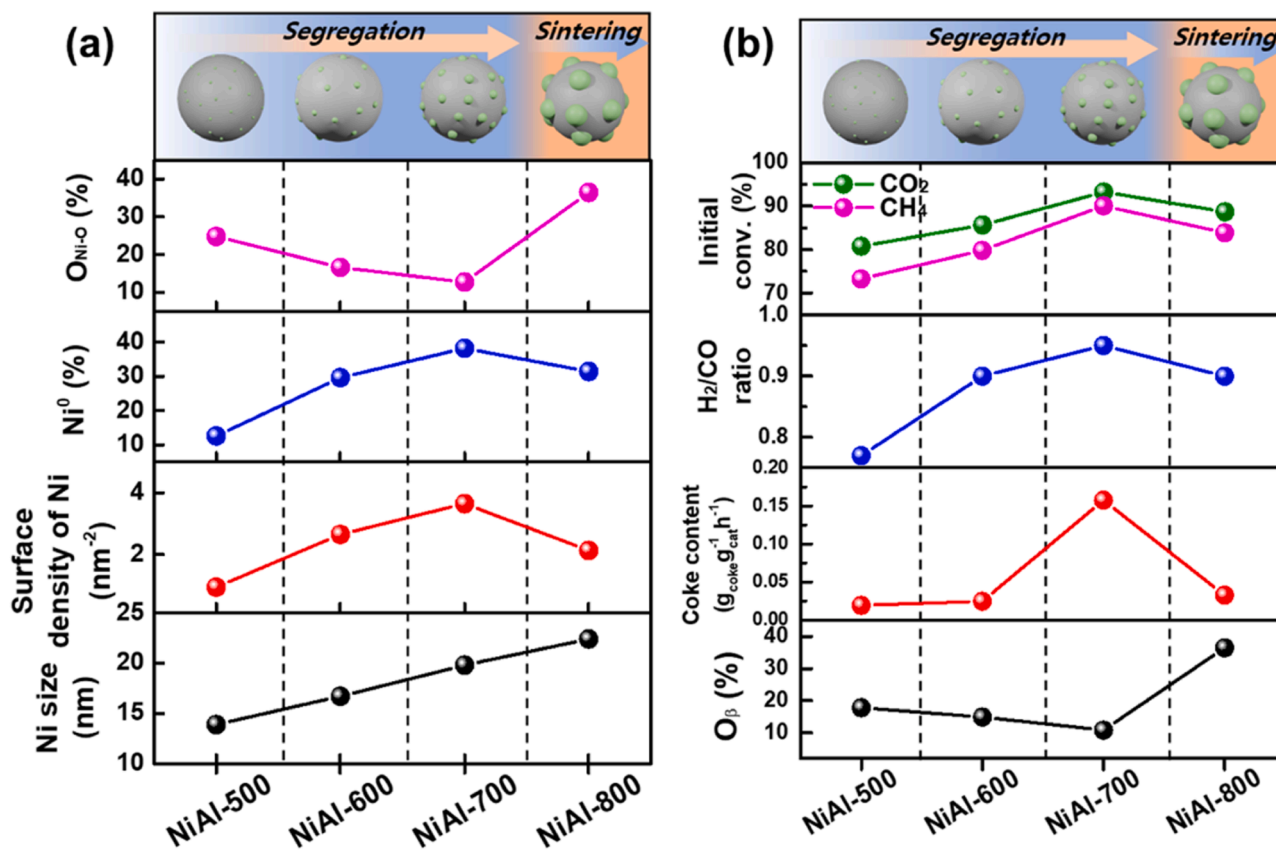
Fig. 6. Relations among physicochemical properties of active sites (a); SEM for average Ni particle size and XPS for relative concentration of Ni^0 and O_{Ni-O}, respectively. Initial CH_4/CO_2 conversions, H_2/CO ratio, coke content, and atomic concentration of O_β over Ni-Al_2O_3 catalysts in DRM reaction (b); Reaction conditions: T = 700°C, CH_4: CO_2 : N_2 = 1:1:1, and WHSV = 180,000 mL$g_{cat}^{-1}h^{-1}$. TGA for coke content and XPS for atomic concentration of O_β.

low O_β concentration was relatively easily deactivated, producing a high content of deposited carbon on the catalyst surface after the DRM reaction.

4. Conclusion

In this work, we synthesized $Ni-Al_2O_3$ DRM catalysts via the spray-pyrolysis-assisted EISA method to systematically investigate catalyst surface change as controlled by composition segregation. In order to induce composition segregation, H_2 pretreatment of the $Ni-Al_2O_3$ catalyst was performed. The result confirmed that segregation in the catalyst had successfully occurred via the post-annealing process and that the segregated Ni nanoparticles were located in different regions of the catalyst particles with simultaneous reduction to metal. Furthermore, it was observed that the size of the Ni nanoparticles on the catalyst surface was highly dependent on the post-annealing temperature. However, the electronic properties did not consistently align with the trend of particle-size growth with post-annealing temperature change. In other words, when the reduction temperature for metal segregation is too high, particle growth on the external surface of the catalyst resulting from post-annealing is no longer due to metal segregation but rather to particle sintering. This phenomenon, as revealed by Ni surface density calculation, directly results in a decreased number of active sites. In order to understand how such a change influences the catalytic reaction, catalyst samples were tested in a DRM reaction. It was confirmed that due to sintering, catalytic performance did not align with the trend of Ni particle-size growth, and further, it was established that initial CH_4/CO_2 conversion is closely linked to Ni surface density. Moreover, NiAl-700 with the low concentration of oxygen vacancies was relatively easily deactivated, producing a high content of deposited carbon on the catalyst surface after the DRM reaction.

This study holds special significance, as it demonstrates that catalytic efficiency is closely associated with Ni surface density rather than with particle size, as observed by composition segregation in the $Ni-Al_2O_3$ catalyst. It will provide valuable insight to future research aimed at developing Ni-based catalysts for DRM reactions.

CRediT authorship contribution statement

Min-Jae Kim: Conceptualization, Investigation, Formal analysis, Visualization, Methodology, Writing – original draft, Writing – Review & editing. **Jeongmin Kim:** Data curation, Investigation, Formal analysis. **Yong Jun Kim:** Data curation, Formal analysis. **Jae-Rang Youn:** Data curation, Formal analysis. **Dong Hyun Kim:** Data curation, Investigation. **Jinghua Guo:** Supervision, Funding acquisition. **Kyubock Lee:** Supervision, Project administration, Funding acquisition, Writing – original draft, Writing – Review & editing.

Declaration of Competing Interest

The authors declare that they have no known competing financial interests or personal relationships that could have appeared to influence the work reported in this paper.

Data Availability

Data will be made available on request.

Acknowledgements

Appendix A. Supporting information

Supplementary data associated with this article can be found in the online version at doi:10.1016/j.jcou.2024.102721.

References

[1] R. Schlögl, Heterogeneous catalysis, Angew. Chem. Int. Ed. (2015), https://doi.org/10.1002/anie.201410738.

[2] M. Campanati, G. Fornasari, A. Vaccari, Fundamentals in the preparation of heterogeneous catalysts, Catal. Today (2003), https://doi.org/10.1016/S0920-5861(02)00375-9.

[3] J.A. Schwarz, C. Contescu, A. Contescu, Methods for preparation of catalytic materials, Chem. Rev. (1995), https://doi.org/10.1021/cr00035a002.

[4] N. Zhang, Q. Shao, X. Xiao, X. Huang, Advanced catalysts derived from composition-segregated platinum-nickel nanostructures: new opportunities and challenges, Adv. Funct. Mater. (2019), https://doi.org/10.1002/adfm.201808161.

[5] F. Tao, M.E. Grass, Y. Zhang, D.R. Butcher, J.R. Renzas, Z. Liu, J.Y. Chung, B.S. Mun, M. Salmeron, G.A. Somorjai, Reaction-driven restructuring of Rh-Pd and Pt-Pd core-shell nanoparticles, Science (2008), https://doi.org/10.1126/science.1164170.

[6] S. Zafeiratos, S. Piccinin, D. Teschner, Alloys in catalysis: phase separation and surface segregation phenomena in response to the reactive environment, Catal. Sci. Technol. (2012), https://doi.org/10.1039/C2CY00487A.

[7] A.J. McCue, J.A. Anderson, CO induced surface segregation as a means of improving surface composition and enhancing performance of CuPd bimetallic catalysts, J. Catal. (2015), https://doi.org/10.1016/j.jcat.2015.06.002.

[8] Z. Niu, N. Becknell, Y. Yu, D. Kim, C. Chen, N. Kornienko, G.A. Somorjai, P. Yang, Nat. Mater. (2016), https://doi.org/10.1038/nmat4724.

[9] X. Liu, A. Wang, L. Li, T. Zhang, C.-Y. Mou, J.-F. Lee, Structural changes of Au-Cu bimetallic catalysts in CO oxidation: in situ XRD, EPR, XANES, and FT-IR characterizations, J. Catal. (2011), https://doi.org/10.1016/j.jcat.2010.12.016.

[10] W.-J. Jang, J.-O. Shim, H.-M. Kim, S.-Y. Yoo, H.-S. Roh, A review on dry reforming of methane in aspect of catalytic properties, Catal. Today (2019), https://doi.org/10.1016/j.cattod.2018.07.032.

[11] Y.-L. Lee, K. Lee, C.H. Ko, H.-S. Roh, Optimization of nano-catalysts for application in compact reformers, Chem. Eng. J. (2022), https://doi.org/10.1016/j.cej.2021.134299.

[12] Y. Wang, J. Peng, C. Zhou, Z.-Y. Lim, C. Wu, S. Ye, W.G. Wang, Effect of Pr addition on the properties of Ni/Al2O3 catalysts with an application in the autothermal reforming of methane, Int. J. Hydrog. Energy (2014), https://doi.org/10.1016/j.ijhydene.2013.10.071.

[13] H. Özdemir, M.A.F. Öksüzömer, M.A. Gürkaynak, Preparation and characterization of Ni based catalysts for the catalytic partial oxidation of methane: effect of support basicity on H2/CO ratio and carbon deposition, Int. J. Hydrog. Energy (2010), https://doi.org/10.1016/j.ijhydene.2010.08.091.

[14] R. López-Fonseca, C. Jiménez-González, B. de Rivas, J.I. Gutiérrez-Ortiz, Partial oxidation of methane to syngas on bulk NiAl2O4 catalyst. Comparison with alumina supported nickel, platinum and rhodium catalysts, Appl. Catal. A: Gen. (2012), https://doi.org/10.1016/j.apcata.2012.06.014.

[15] C. Jiménez-González, Z. Boukha, B. de Rivas, J.J. Delgado, M.Á. Cauqui, J.R. González-Velasco, J.I. Gutiérrez-Ortiz, R. López-Fonseca, Structural characterization of Ni/alumina reforming catalysts activated at high temperatures, Appl. Catal. A: Gen. (2013), https://doi.org/10.1016/j.apcata.2013.06.017.

[16] K. Okuyama, I.W. Lenggoro, Preparation of nanoparticles via spray route, Chem. Eng. Sci. (2003), https://doi.org/10.1016/S0009-2509(02)00578-X.

[17] P.S. Patil, Versatility of chemical spray pyrolysis technique, Mater. Chem., Phys. (1999), https://doi.org/10.1016/S0254-0584(99)00049-8.

[18] M.-J. Kim, J.-R. Youn, H.J. Kim, M.W. Seo, D. Lee, K.S. Go, K.B. Lee, S.G. Jeon, Effect of surface properties controlled by Ce addition on CO2 methanation over Ni/Ce/Al2O3 catalyst, Int. J. Hydrog. Energy (2020), https://doi.org/10.1016/j.ijhydene.2020.06.144.

[19] J.-C. Seo, E. Cho, J. Kim, S.B. Kim, J.-R. Youn, D.H. Kim, P.K. Ramasamy, K. Lee, C.H. Ko, Bifunctional metal doping engineering of Ni-supported alumina catalyst for dry methane reforming, J. Environ. Chem. Eng. (2022), https://doi.org/10.1016/j.jece.2022.108058.

[20] T. Rajkumar, A. Sápi, M. Ábel, F. Farkas, J.F. Gómez-Pérez, Á. Kukovecz, Z. Kónya, Ni-Zn-Al-based oxide/spinel nanostructures for high performance, methane-selective CO2 hydrogenation reactions, Catal. Lett. (2020), https://doi.org/10.1007/s10562-019-03051-8.

[21] M. Luo, S. Guo, Strain-controlled electrocatalysis on multimetallic nanomaterials, Nat. Rev. Mater. (2017), https://doi.org/10.1038/natrevmats.2017.59.

[22] S. Zhang, X. Zhang, G. Jiang, H. Zhu, S. Guo, D. Su, G. Lu, S. Sun, Tuning nanoparticle structure and surface strain for catalysis optimization, J. Am. Chem. Soc. (2014), https://doi.org/10.1021/ja5030172.

[23] D. Beierlein, D. Häussermann, M. Pfeifer, T. Schwarz, K. Stöwe, Y. Traa, E. Klemm, Is the CO2 methanation on highly loaded Ni-Al2O3 catalysts really structure-sensitive? Appl. Catal. B: Environ. (2019) https://doi.org/10.1016/j.apcatb.2018.12.064.

[24] D.H. Kim, J.-R. Youn, J.-C. Seo, S.B. Kim, M.-J. Kim, K. Lee, One-pot synthesis of NiCo/MgAl$_2$O$_4$ catalyst for high coke-resistance in steam methane reforming: optimization of Ni/Co ratio, Catal. Today (2023), https://doi.org/10.1016/j.cattod.2022.09.016.

[25] D.A. Pawlak, K. Woźniak, Z. Frukacz, T.L. Barr, D. Fiorentino, S. Seal, ESCA studies of yttrium aluminum garnets, J. Phys. Chem. B (1999), https://doi.org/10.1021/jp9838801.

[26] W. Zha, Z. Zhou, D. Zhao, S. Feng, Positive effects of Al^{3+} partially substituted by Co^{2+} cations on the catalytic performance of Co$_{1+x}$Al$_{2-x}$O$_4$ (x=0-0.2) for methane combustion, J. Sol. -Gel Sci. Technol. (2016), https://doi.org/10.1007/s10971-015-3910-2.

[27] N.F.M. Salleh, A.A. Jalil, S. Triwahyono, J. Efendi, R.R. Mukti, B.H. Hameed, New insight into electrochemical-induced synthesis of NiAl$_2$O$_4$/Al$_2$O$_3$: synergistic effect of surface hydroxyl groups and magnetism for enhanced adsorptivity of Pd (II), Appl. Surf. Sci. (2015), https://doi.org/10.1016/j.apsusc.2015.05.048.

[28] J. Jun, M. Dhayal, J.-H. Shin, Y.H. Han, N. Getoff, Surface chemistry and catalytic activity of Ni/Al$_2$O$_3$ irradiated with high-energy electron beam, Appl. Surf. Sci. (2008), https://doi.org/10.1016/j.apsusc.2008.01.048.

[29] Z. Boukha, C. Jiménez-González, B. de Rivas, J.R. González-Velasco, J.I. Gutiérrez-Ortiz, R. López-Fonseca, Synthesis, characterization and performance evaluation of spinel-derived Ni/Al$_2$O$_3$ catalysts for various methane reforming reactions, Appl. Catal. B: Environ. (2014), https://doi.org/10.1016/j.apcatb.2014.04.014.

[30] M. Gil-Calvo, C. Jiménez-González, B. de Rivas, J.I. Gutiérrez-Ortiz, R. López-Fonseca, Effect of Ni/Al molar ratio on the performance of substoichiometric NiAl$_2$O$_4$ spinel-based catalysts for partial oxidation of methane, Appl. Catal. B: Environ. (2017), https://doi.org/10.1016/j.apcatb.2017.02.063.

[31] R. Patel, A.H. Fakeeha, S.O. Kasim, M.L. Sofiu, A.A. Ibrahim, A.E. Abasaeed, R. Kumar, A.S. Al-Fatesh, Optimizing yttria-zirconia proportions in Ni supported catalyst system for H$_2$ production through dry reforming of methane, Mol. Catal. (2021), https://doi.org/10.1016/j.mcat.2021.111676.

[32] L. Pino, C. Italiano, A. Vita, M. Laganà, V. Recupero, Ce$_{0.70}$La$_{0.20}$Ni$_{0.10}$O$_{2-\delta}$ catalyst for methane dry reforming: influence of reduction temperature on the catalytic activity and stability, Appl. Catal. B: Environ. (2017), https://doi.org/10.1016/j.apcatb.2017.06.080.

[33] G. Garbarino, C. Wang, I. Valsamakis, S. Chitsazan, P. Riani, E. Finocchio, M. Flytzani-Stephanopoulos, G. Busca, A study of Ni/Al$_2$O$_3$ and Ni-La/Al$_2$O$_3$ catalysts for the steam reforming of ethanol and phenol, Appl. Catal. B: Environ. (2015), https://doi.org/10.1016/j.apcatb.2015.02.024.

[34] S.-H. Cai, S.N. Rashkeev, S.T. Pantelides, K. Sohlberg, Atomic scale mechanism of the transformation of γ-alumina to θ-alumina, Phys. Rev. Lett. (2002), https://doi.org/10.1103/PhysRevLett.89.235501.

[35] D.W. Kwon, K.H. Park, S.C. Hong, Influence of VO$_x$ surface density and vanadyl species on the selective catalytic reduction of NO by NH$_3$ over VO$_x$/TiO$_2$ for superior catalytic activity, Appl. Catal. A: Gen. (2015), https://doi.org/10.1016/j.apcata.2015.04.005.

[36] Y.-L. Lee, K.-J. Kim, W.-J. Jang, J.-H. Shim, K.-W. Jeon, H.-S. Na, H.-M. Kim, J.W. Bae, S.C. Nam, B.-H. Jeon, H.-S. Roh, Increase in stability of BaCo/CeO$_2$ catalyst by optimizing the loading amount of Ba promoter for high-temperature water-gas shift reaction using waste-derived synthesis gas, Renew. Energy (2020), https://doi.org/10.1016/j.renene.2019.08.050.